14th International Conference on Turbochargers and Turbocharging
Institution of Mechanical Engineers, ISBN: 978-0-367-67645-2

Multidisciplinary and multi-point optimisation of radial and mixed-inflow turbines for turbochargers using 3D inverse design method

J. Zhang

Advanced Design Technology Ltd, UK

M. Zangeneh

Department of Mechanical Engineering, University College London, UK

ABSTRACT

The radial and mixed-inflow turbines have been widely used for the turbocharger application. The design of a turbocharger turbine with good performance still presents a lot of challenges. Apart from the traditional requirements such as high efficiency and low stress, the turbine blade is also required to achieve certain performance targets at multiple operating points, high unsteady efficiency under pulsating flow condition, reduced moment of inertia (MOI) and high vibration characteristic. To meet these challenges, it is important to optimise the radial and mixed-inflow turbines for the aerodynamic performance at multiple operating points and the structural performance subject to MOI, stress and vibration constraints. In this paper we propose an approach based on 3D inverse design method that makes such a design optimisation strategy possible under industrial timescales. Using the inverse design method, the turbine blade geometry is computed iteratively based on the prescribed blade loading distribution. The radial filament blading is always applied by the conventional design method to reduce the stress, while the inverse designed blade is three-dimensional (3D). A radial filament modification method is proposed to control the stress level of 3D blades. The turbine's aerodynamic and mechanical performance is evaluated using CFD (5 operating points) and Finite Element Analysis (FEA). A linear regression is performed based on the results of the linear DOE study. The number of design parameters is reduced based on a sensitivity analysis of the linear polynomial coefficients. A more detailed DOE with around 60 designs is generated and Kriging is used to construct a response surface model (RSM). Multi-objective genetic algorithm (MOGA) is then used to search the optimal designs which meet multiple constraints and objectives on the Kriging response surface. The performance of the final optimal design is evaluated in both the aerodynamic and mechanical aspects based on CFD and FEA simulations. The numerical results show that the optimal design leads to better performance in almost all aspects including improved efficiency in the design point and high U/C_{is} (velocity ratio), similar maximum stress, reduced MOI and increased vibration frequencies.

1 INTRODUCTION

The main challenge for the multidisciplinary and multi-objective optimisation of turbomachinery blades are the time-consuming meshing, CFD, static structural and modal analysis which require a tremendous amount of computational resources (CPU time and computer memory). To accelerate and improve the optimisation process, surrogate models have been widely used. The terms surrogate model, approximation model, response surface and metamodel are used as synonym in the literature. The surrogate model is constructed based on data from known designs (usually from DOE) and provides fast approximation and evaluation of objectives for different design parameters at new design points. The most commonly used surrogate models are polynomial approximation [1-5], artificial neural network (ANN) or radial basis function (RBF) [6-11] and Kriging [12-13]. A detailed review of these methods can be found in Queipo et al [14].

In this paper, first-order (linear) polynomial, Kriging approximation and inverse design method will be used to optimise the aerodynamic and mechanical performance of a turbocharger turbine.

2 OPTIMISATION METHODOLOGY

The flowchart of the optimisation methodology used in this paper is shown in Figure 1.

To generate a blade geometry using the inverse design method, the meridional geometry, the thickness distribution and the blade loading distribution are necessary inputs. The parametrisation of all these outputs and their ranges of the variation have to be specified first during the optimisation process. The output parameters including the aerodynamic performance parameters and the mechanical performance parameters of any designs in the optimisation will be evaluated using CFD and FEA.

A linear DOE and RSM model are generated based on the design parameters and performance parameters using first-order polynomial regression. The number of the design parameters is reduced based on the sensitivity analysis which compares the normalised coefficients of the linear polynomial and the most significant design parameters are selected whose variation have a larger effect on the performance parameters.

A new DOE with more designs is then generated for the new selected design parameters and their performance parameters are evaluated using CFD and FEA simulations. The Kriging approximation is used to build the Kriging RSM based on the new DOE results.

Finally a Pareto front is generated through searching the optimal designs on the Kriging RSM quickly using MOGA and several optimal designs can be selected from the Pareto front. The performance parameters of these optimal designs are validated against CFD and FEA calculations.

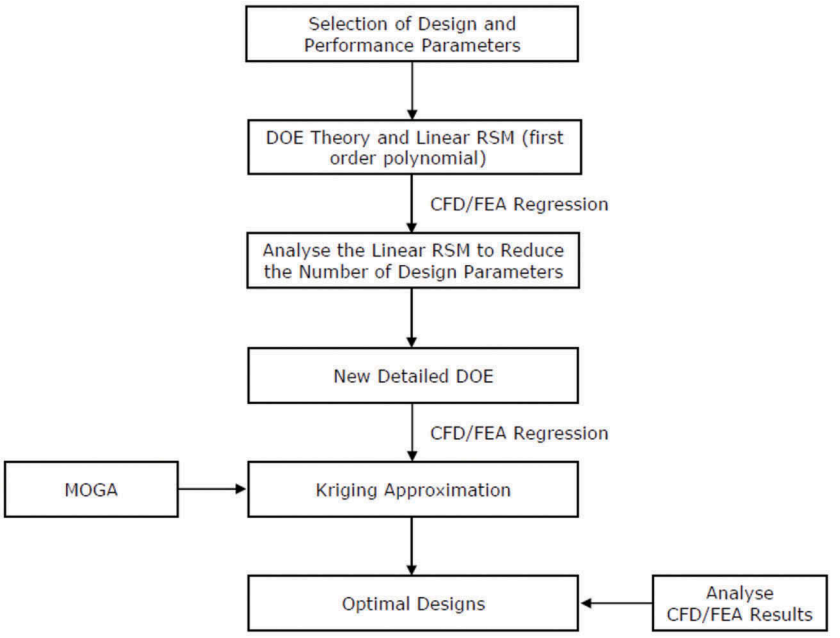

Figure 1. Flowchart of the optimisation methodology.

3 BLADE PARAMETERISATION

The design parameters consist of 6 meridional geometry parameters, 10 blade loading parameters and 1 thickness parameter.

It is shown in Figure 2 that the five control points A, B, C, D and E are used to create the hub curve and the shroud curve is created similarly using A', B', C', D' and E'. Both hub and shroud curves are created by the cubic spline method. The radial coordinate of point B' (maximum tip radius) is fixed (38 mm) while the axial coordinate of point B is also fixed (0 mm). Point D is fixed in both axial and radial directions to make sure all the blades have the same blade length and shaft radius as the baseline. The 6 design parameters used to define the blade meridional geometry are the inducer width W_1, the exducer width W_2, the LE angle α_1, the TE angle α_2, the hub and shroud control points Y_{hub} and Y_{shr}.

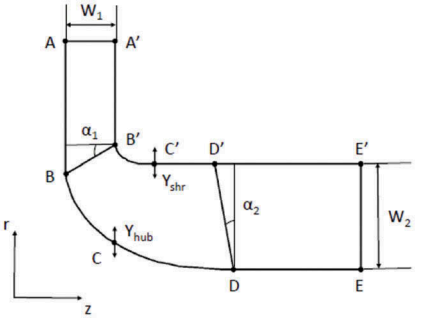

Figure 2. Meridional plane parameters.

The blade shape is computed iteratively based on prescribed blade loading using inverse design method. The blade loading is defined by LE/TE rV_θ and the derivative of rV_θ along the meridional direction ($\partial rV_\theta/\partial m$). The streamwise blade loading ($\partial rV_\theta/\partial m$) is defined by a three-segment method (more details can be found in [15]). The 10 blade loading parameters are $rV_{\theta TE,hub}$, $rV_{\theta TE,shr}$, NC_{hub}, NC_{shr}, ND_{hub}, ND_{shr}, $SLOPE_{hub}$, $SLOPE_{shr}$, $DRVT_{LE,hub}$ and $DRVT_{LE,shr}$.

The blade thickness is controlled by one non-dimensional factor called thickness parameters which is greater than 0.9 and less than 1.2. The shroud thickness of the blade remains the same and the hub thickness is multiplied by the thickness parameter. The thickness between the hub and the shroud sections is recalculated through linear interpolation.

3D radial turbine blades designed using the inverse design method show 2-3% higher efficiency than the conventional radial fibre design (validated against numerical and experimental results by Zangeneh-Kazemi [16]). However, their stress values are much higher than the material strength. To reduce the stress level of the 3D blades, a blade modification method called Radial Filament Modification method 1 (RFM1) is introduced. Basically, the wrap angle distribution at the LE and shroud of the blade remains the same and are mapped radially to all the other part of the blades. By doing this, the stress level of 3D blades will be reduced significantly.

For an optimisation process, it is desirable to explore the design space as much as possible, this requires a wide variation of all the design parameters in order to increase the change that the global optimal design can be found. However, if the range of design parameters is too big, a large number of poor designs have to be evaluated which will significantly increase the complexity and the cost of the optimisation process. Therefore, the range of all the 17 design parameters are carefully selected and are shown in Table 1.

Table 1. Variation ranges of design parameters.

Design parameter	Min	Max
W_1 (mm)	7	11
W_2 (mm)	15	24
σ_1	0°	40°
σ_2	0°	10°
Y_{hub} (mm)	16.5	21
Y_{shr}	0.2	0.4
$rV_{\theta TE,hub}$	0	0.04
$rV_{\theta TE,shr}$	0.06	0.1
NC_{hub}	0.05	0.2
NC_{shr}	0.05	0.4
ND_{hub}	0.6	0.85
ND_{shr}	0.6	0.85
$Slope_{hub}$	1	2.5
$Slope_{shr}$	-5	-1
$DRVT_{LE,hub}$	-1	-0.1
$DRVT_{LE,shr}$	-1	-0.1
Thickness	0.9	1.2

4 STEADY CFD ANALYSIS

The computational domain used for the steady CFD simulation is shown in Figure 3. The nozzle mesh is unstructured and generated using ANSYS Meshing. The inflation layers are applied on all the nozzle walls with a near wall element distance of 0.001 mm to capture the boundary layer effects. The rotor mesh is structured (hexahedron) and generated using ANSYS TurboGrid. The first element offset is also 0.001 mm. There are 20 layers of elements in the shroud clearance whose value is 0.5 mm. The total number of elements is around 2,200,000.

The nozzle domain is stationary and the rotor domain is rotating with a constant speed. Inlet boundary conditions are total pressure and total temperature. Inlet absolute flow angle is 40° from the tangential direction which is determined by a given volute geometry. Outlet boundary condition is atmospheric static pressure (1.0 bar). Rotational periodical boundary conditions are applied on all the periodic surfaces of the nozzle and rotor domains. The Stage (or mixing plane) method is used for the interface between the stator and the rotor. The Stage model performs a circumferential averaging of the fluxes through the interface and passes it to the component downstream. The turbulence model used is the shear stress transport (SST) k-ω. The working fluid is assumed to be ideal gas with gamma = 1.4. RANS equations are solved iteratively to obtain the whole flow field. T-S Efficiency (η_{50k}, η_{60k}, η_{70k}, η_{80k} and η_{90k}) and turbine mass flow parameter (MFP_{50k}, MFP_{60k}, MFP_{70k}, MFP_{80k}, MFP_{90k}) for five different RPM are used to evaluate the turbine aerodynamics performance and flow capacity.

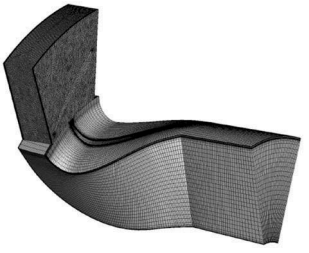

Figure 3. CFD computational domain.

5 STATIC STRUCTURAL AND MODAL ANALYSIS

The blade geometry used in the steady CFD simulation is just a single blade which is not enough for the static structural and the modal analysis of the turbine wheel. To get accurate evaluation of the stress value and vibration characteristics during the turbine's rotation it is necessary to create the whole turbine wheel geometry from the single turbine blade by using Pro/ENGINEER which is a commercial CAD software now known as PTC Creo. Variable radius fillet is generated between the blade root and the hub to reduce the stress concentration. The minimum fillet radius has to be greater than 1mm due to the manufacture restrictions and the adjacent fillets must not contact each other. To reduce the MOI of the rotor the back face is scalloped by removing metal between the blades in the inducer region, which will reduce the turbine efficiency by ~1-3%.

The mesh is generated by using ANSYS Meshing as shown in Figure 4. And the total number of unstructured elements is around 150,000. Only one blade mesh is refined (element size = 0.6 mm) to save computational resources and time since the whole wheel geometry is axisymmetric. The mesh in the hub fillet and the blade trailing edge is refined further (element size = 0.3 mm) since they are locations where the maximum stress occurs.

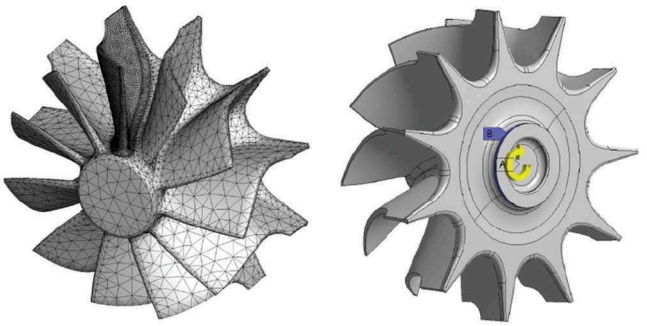

Figure 4. Mesh and boundary conditions for FEA.

The material used to manufacture the turbine is Inconel 713C. The wheel MOI can be obtained directly through ANSYS Mechanical once the geometry is imported. For the static structural analysis, the boundary conditions applied are the rotational velocity (A in Figure 4) and the cylindrical support (B in Figure 4) provided by the shaft connected to the compressor. The rotating speed is 130,000 rev/min which is the maximum working speed of the turbine. For the model analysis, the boundary condition applied is only the cylindrical support without pre-stress consideration.

The turbine mechanical performance parameters including the maximum principle stress, 1st and 2nd model natural frequencies and MOI will be obtained.

6 LINEAR DOE AND SENSITIVITY STUDY

The 25 design points are generated for the 17 design parameters with 25 different levels (the ranges specified in Table 1) using OLHS and allow several designs to diverge and fail to create geometries. Finally 19 designs converge and generate blade geometries using the inverse design method which is sufficient for the linear regression. The design matrix including the design parameters and the performance parameters of all 19 designs is called the linear DOE.

To reduce the number of design parameters (n = 17), a sensitivity analysis is performed by comparing the value of normalised polynomial coefficient $(\hat{a}_i^j)$ which is shown in Equation (1). Where $\hat{x}_i$ is the ith design parameter (normalised to 0-1) and $\hat{y}_j$ is the jth performance parameter (normalised to 0-1).

$$\hat{y}_j = \hat{a}_0^j + \sum_{i=1}^{17} \hat{a}_i^j \hat{x}_i \tag{1}$$

The normalised coefficients $\tilde{A}_i^j$ is defined by Equation (2). The range of $\tilde{A}_i^j$ is from -100 to 100. For a particular performance parameter y_j (j is constant), the greater the absolute value of $\tilde{A}_i^j$ is, the more significant the corresponding design parameter x_i is.

$$\tilde{A}_i^j = \frac{\hat{a}_i^j}{\max\left(\left|\hat{a}_i^j\right|\right)} \times 100 \tag{2}$$

The most significant design parameters are selected based on the summation of all the absolute values of $\tilde{A}_i^j$. The number of the significant parameters selected is directly related to the size (or the dimension) of the design space and the computational cost. The larger this number is, the more likely the optimal design can be found while more sampling points and computational resource are needed. Therefore, the 8 most significant design parameters are selected which are W_2, W_1, α_1, NC_{hub}, Y_{hub}, ND_{hub}, $SLOPE_{shr}$ and $rV_{\theta TE,shr.}$ The variation of these 8 design parameters have much larger effect on the performance parameters compared to the other design parameters. Different weighting numbers can be applied for different performance parameters during this summation process and this will result in different collections of most significant design parameters. In this study the weighting numbers for different performance parameters are assumed to be identical.

7 KRIGING APPROXIMATION AND MOGA OPTIMISATION

In the previous section, the number of design parameters has been successfully reduced from 17 to 8 by a sensitivity analysis based on the linear DOE results. A more accurate approximation method (Kriging) will be used for these new 8 design parameters and MOGA will be used to search the design space to obtain the optimal design which meets multiple objectives and constraints.

The accuracy of the Kriging RSM is directly related to the number of the sampling points and the sampling method. The more points are used to build the Kriging RSM, the more accurate the model will be. In total 60 designs are generated by the OLHS method for the 8 new selected design parameters. The values of other design parameters are set as medial value or same as the baseline value since they have little effect on the performance parameters. The 53 of 60 designs converge and generate blade geometries using the inverse design method. Radial Filament Modification method 1 is performed for these 53 blade geometries to get RFM1 blades. CFD and FEA calculations are run for these 53 new RFM1 blades. A Kriging RSM then can be constructed using the design and performance parameters of these 53 designs. The performance parameters of any new designs in the optimisation can be evaluated quickly through the Kriging RSM instead of the expensive CFD and FEA simulations.

The constraints used in the optimisation are summarised in Table 2. The objectives are to maximise η_{70k} and minimise Stress. The flow chart of MOGA optimisation based on RSM is illustrated in Figure 5. NSGA-II is used to search the design space based on the constraints and objectives specified above. The performance parameters are evaluated through the Kriging approximation model which is much faster compared to the time consuming CFD and FEA simulations. The population size is set as 100 and the number of generations is set as 120. In total 12,000 designs are generated and their aerodynamic and mechanical performance values can be evaluated in 10 minutes.

Table 2. Constraints used in the optimisation.

	Constraints
η_{50k}	> 0.599
η_{60k}	> 0.665
η_{80k}	> 0.633
η_{90k}	> 0.547
MFP_{50k}	> 23.3
1st freq	> 7479
2nd freq	> 13535
MOI	< 8.8342×10^{-5}

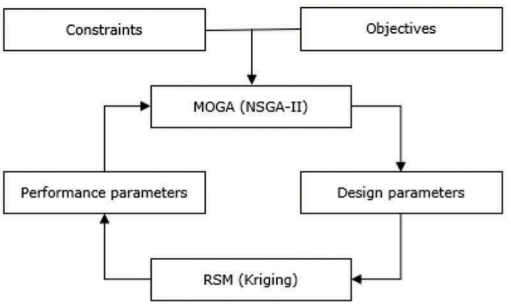

Figure 5. The flow chart of MOGA optimisation based on RSM.

A Pareto front is plotted in Figure 6. The Stress value is normalised by a constant value. Three optimal designs (design 5571, 7222 and 10535) are selected from the Pareto Font and their performance parameters are validated by CFD and FEA simulations. The comparison of performance improvements for design 5571, design 7222 and design 10535 compared to the baseline is shown in Figure 7. As it can be seen that design 5571 has the best efficiency but wor.st mechanical performance. Design 7222 has the best mechanical performance but worst efficiency. A clear trade-off between the aerodynamic performance and the mechanical performance is demonstrated. The error between the prediction value and CFD/FEA validation value for most of the performance parameters are between 0.8 and 4.4%. Design 10535 is selected and further analysis will be performed in the following section.

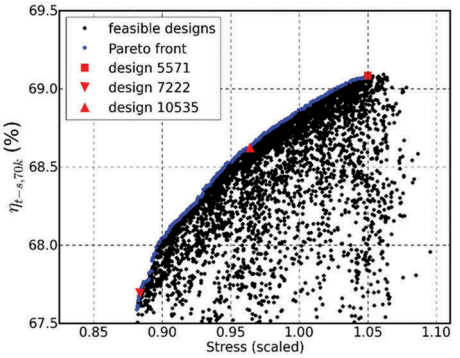

Figure 6. 2D scatter plot of η_{70k} versus Stress (scaled) for Kriging approximation.

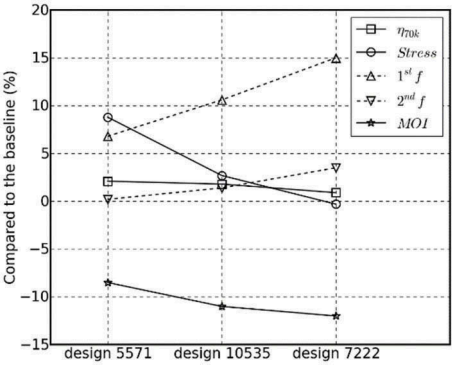

Figure 7. Comparison of performance improvements for design 5571, design 7222 and design 10535.

8 RESULTS

8.1 Comparison of meridional geometry and performance maps

The meridional geometry comparison between the baseline and design 10535 is shown in Figure 8. As it can be seen that the most obvious differences for design 10535 are the increased α_1 and reduced W_2 which are helpful to reduce MOI. The reduced blade exducer height W_2 of design 10535 is helpful to increase the blade stiffness. The MFP and $\eta_{t\text{-}s}$ comparison of the baseline and design 10535 are shown in Figure 9. The MFP of design 10535 is slightly higher at $U/C_{is} < 0.6$ and slightly lower at $U/C_{is} > 0.6$ compared to the baseline. The $\eta_{t\text{-}s}$ of design 10535 at $U/C_{is} < 0.64$ keeps almost the same as the baseline and is much higher (up to 5 percentage points) at $U/C_{is} > 0.64$.

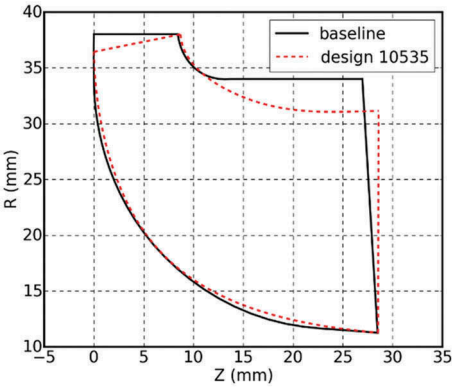

Figure 8. Comparison of meridional geometries.

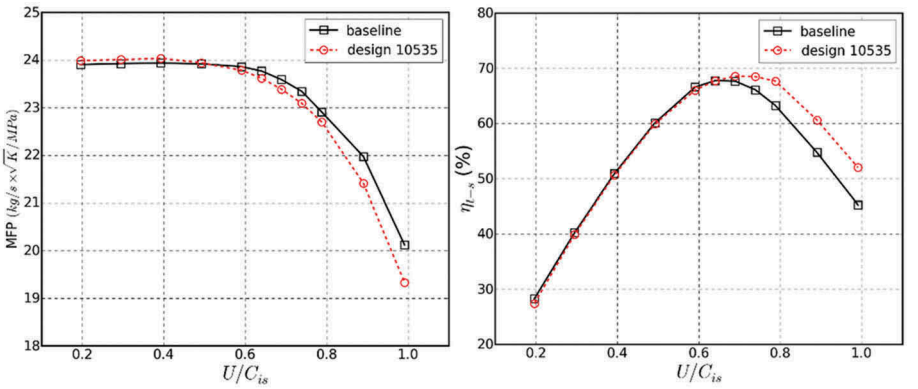

Figure 9. Comparison of MFP and t-s efficiency.

8.2 Comparison of internal flow field

In this subsection, the internal flow field details of the baseline and design 10535 at RPM = 80k (U/C_{is} = 0.79) where the efficiency improvement is much higher than that at design point (RPM = 70k).

The blade surface (suction side) streamlines comparison for the two designs is shown in Figure 10. One can see that design 10535 has a much better streamline distribution attached on the blade surface, since it has less secondary flow whose direction is from the hub to the shroud compared to the baseline.

The streamlines for the tip leakage flow for these two designs are compared in Figure 11. It can be seen that most of the tip leakage flow starts from the blade LE pressure side. The flow direction is from the pressure side to the suction side along the whole chord locations from the LE to the TE. A small leakage vortex is generated near the LE suction side and this vortex grows and mixes with any new leakage flow from the pressure side along the meridional direction. Design 10535 has a better leakage flow structure since the strength of the leakage vortex and its entropy generation for design 10535 is smaller than the baseline which can be seen in Figure 12.

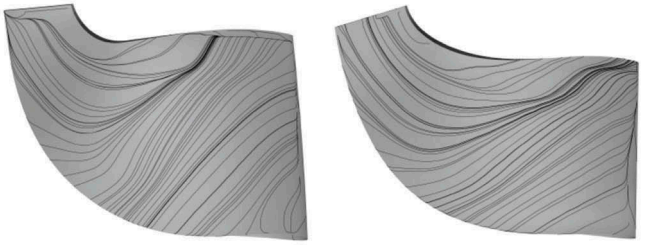

Figure 10. Comparison of blade surface streamlines on the suction side @ RPM = 80k (left – baseline, right – design 10535).

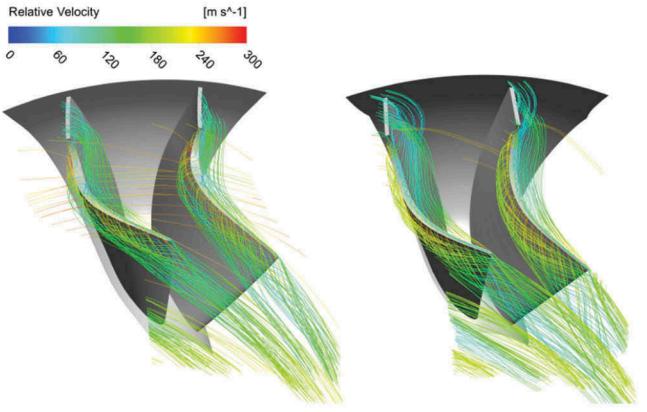

Figure 11. Comparison of streamlines across the tip leakage @ RPM = 80k (left – baseline, right – design 10535).

The comparison of static entropy contours for the two designs at three different streamwise locations is shown in Figure 12 and the last section is located at the TE. As it can be seen that most of the entropy is accumulated near the blade tip suction side where the tip leakage vortex locates. At the same streamwise location, the baseline has higher entropy than design 10535. Especially, in the TE, the baseline has two high entropy regions near the tip while 10535 only has one.

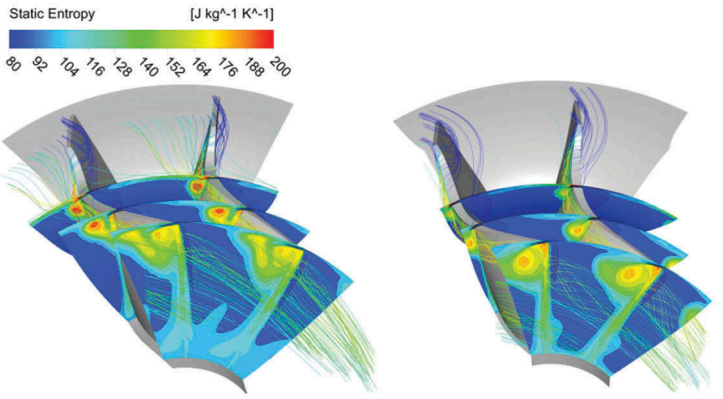

Figure 12. Comparison of streamlines associated with static entropy contours at different streamwise locations @ RPM = 80k (left – baseline, right – design 10535).

8.3 Comparison of static structural and modal analysis results

The comparison of stress contours for the two designs is shown in Figure 13. The stress distribution on the blade surface are very similar for these two designs. The stress level in the hub fillet of design 10535 is reduced compared to the baseline. The maximum stress occurs in the same location which is in the TE hub region. The maximum stress of design 10535 is 2.3% higher than the baseline and this can be easily reduced by increasing the fillet radius slightly near the TE. The frequency for 1st vibration mode of design 10535 is 10.6% higher than the baseline and the frequency for 2nd vibration mode of design 10535 is 1.4% higher than the baseline.

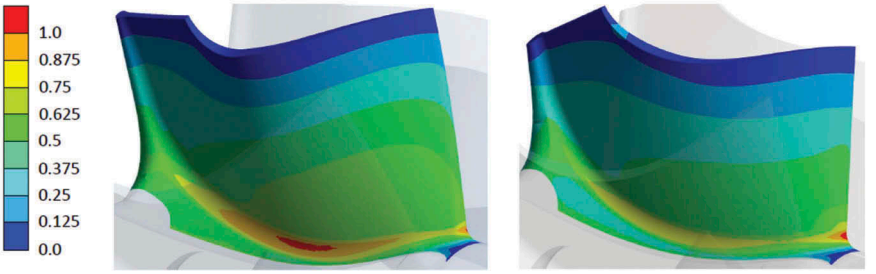

Figure 13. Comparison of maximum principle stress (scaled) contours on the suction surface (left – baseline, right – design 10535).

9 CONCLUSIONS

A systematic optimisation methodology using the inverse design method, DOE, RFM1, Kriging approximation and MOGA is presented in this paper. The inverse design method is used to generate the 3D blade geometry and Radial Filament Modification method 1 is used to modify the 3D blade shape to reduce the maximum stress. The number of

design parameters is reduced from 17 to 8 through a sensitivity analysis based on the linear DOE results. The Kriging is used to construct a more accurate response surface for the new selected design parameters. An optimal design, design 10535, is obtained by searching on the Kriging RSM using MOGA with multiple constraints and objectives. Design 10535 shows better aerodynamic and mechanical performance compared to the baseline design, especially the efficiency at high U/C_{is} and MOI (-11.0%). The improved performance of design 10535 is confirmed by detailed CFD and FEA analysis.

The inlet to a turbocharger turbine encounters highly unsteady flow with varying pressure and temperature due to the pulsating nature of the exhaust gas from the internal combustion engine. It is very important to improve the cycle-averaged t-s efficiency which enables turbines to extract more energy from the exhaust gas during one pulse cycle. The pulsating engine exhaust gas with high pressure and temperature (low U/C_{is} region) carries more energy than high U/C_{is} region. Therefore, it is suggested that future work should involve improving the turbine efficiency at low U/C_{is} region while maintaining low MOI and stress.

ACKNOWLEDGEMENTS

This research is sponsored by Cummins Turbo Technologies and EPSRC. The author would like to thank their financial support.

NOMENCLATURE

ANN	artificial neural network
CFD	computational fluid dynamics
DOE	design of experiment
DRVT	streamwise blade loading parameter
FEA	finite element analysis
LE	leading edge
MFP	mass flow parameter
MOGA	multi-objective genetic algorithm
MOI	moment of inertia
NC	streamwise blade loading parameter
ND	streamwise blade loading parameter
OLHS	optimal Latin hypercube sampling
RANS	Reynolds-averaged Navier–Stokes
RBF	radial basis function
RFM1	radial filament modification method 1
RSM	response surface model
SLOPE	streamwise blade loading parameter

(*Continued*)

(*Continued*)

SST	shear stress transport
TE	trailing edge
a	polynomial coefficient
m	meridional coordinate
rV_θ	swirl velocity
U/C_{is}	velocity ratio
W_1	inducer width
W_2	exducer width
x:	design parameter
y:	performance parameter
Y_{hub}	hub control point
Y_{shr}	shroud control point
α_1	LE angle
α_2	TE angle
η	efficiency

REFERENCES

[1] Dornberger, R., Buche, D. & Stoll, P. 2000. *Multidisciplinary Optimization in Turbomachinery Design*. European Congress on Computational Methods in Applied Sciences and Engineering.

[2] Lian, Y. & Liou, M. 2005. *Multiobjective Optimization Using Coupled Response Surface Model and Evolutionary Algorithm*. AIAA Journal.

[3] Goel, T., Vaidyanatham, R., Haftka, R. T., Shyy, W., Queipo, N. V. & Tucker, K. 2007. *Response Surface Approximation of Pareto Optimal Front in Multi-objective Optimization*. Computer Methods in Applied Mechanics and Engineering, 196:879–893.

[4] Bonataki, E. & Zangeneh, M. 2009. *On the Coupling of Inverse Design and Optimization Techniques for the Multi-objective, Multipoint Design of Turbomachinery Blades*. Journal of Turbomachinery, 131(2):021014.

[5] Kim, J-H, Choi, J-H, Husain, A. & Kim, K-Y. 2010. *Performance Enhancement of Axial fan Blade through Multi-objective Optimisation Techniques*. Journal of Mechanical Science and Technology, 24(10):2059–2066.

[6] Verstraete, T., Alsalihi, Z. & Van den Braembussche, R. A. 2007. *Multidisciplinary Optimization of A Radial Compressor for Micro Gas Turbine Applications*. Journal of Turbomachinery, 132(3):031004.

[7] Pierret, P. 2005. *Multi-objective Optimization of Three Dimensional Turbomachinery Blades*. European Conference for Aerospace Sciences.

[8] Pierret, P., Filomeno Coelho, R. & Kato, H. 2007. *Multidisciplinary and Multiple Operating Points Shape Optimization of Three-dimensional Compressor Blades*. Structural and Multidisciplinary Optimization, 33(1):61–70.

[9] Roclawski, H., Bohle, M. & Gugau, M. 2012. *Multidisciplinary Design Optimization of A Mixed Flow Turbine Wheel*. ASME Turbo Expo 2012, GT2012-68233:499-509.

[10] Chahine, C., Seume, J. R. & Verstraete, T. 2012. *The Influence of Metamodeling Techniques on the Multidisciplinary Design Optimization of A Radial Compressor Impeller*. ASME Turbo Expo 2012, GT2012-68358:1951–1964.
[11] Mueller, L., Alsalihi, Z. & Verstraete, T. 2013. *Multidisciplinary Optimization of A Turbocharger Radial Turbine*. Journal of Turbomachinery, 135(2):021022.
[12] Chung, H-S & Alonso, J. J. 2004. *Multiobjective Optimization Using Approximation Model-based Genetic Algorithms*. 10th AIAA/ISSMO Symposium on Multidisciplinary Analysis and Optimization.
[13] Siller, U., Vob, C. & Nicke, E. 2009. *Automated Multidisciplinary Optimization of A Transonic Axial Compressor*. 47th AIAA Aerospace Sciences Meeting including the New Horizons Forum and Aerospace Exposition.
[14] Queipo, N. V., Haftka, R. T., Shyy, W., Goel, T., Vaidyanathan, R. & Tucker, P. K. 2005. *Surrogate-based Analysis and Optimization*. Progress in Aerospace Sciences, 41(1):1–28.
[15] Zhang, J., Zangeneh, M. & Eynon, P. 2014. *A 3D Inverse Design based Multidisciplinary Optimization on the Radial and Mixed-inflow Turbines for Turbochargers*. IMechE 11th International Conference on Turbochargers and Turbocharging, pages 399–410.
[16] Zangeneh-Kazemi, M. 1986. *Three-Dimensional Design of Radial-Inflow Turbines*. PhD thesis, Cambridge University, Engineering Department.